On the Plausibility of Thermodiffusion as the Primary Mechanism for Unipolar Resistive Switching in Metal-Oxide-Metal Memristive Devices

Kristof Lange
Institut für Werkstoffe der Elektrotechnik II (IWE2)
RWTH Aachen University
Aachen, Germany
0009-0001-4172-3534

Rainer Waser
Institut für Werkstoffe der Elektrotechnik II (IWE2)
RWTH Aachen University
Aachen, Germany
0000-0002-5426-9967

Stephan Menzel
Peter Grünberg Institut (PGI-7)
Forschungszentrum Jülich GmbH
Jülich, Germany
0000-0002-4258-2673

***Abstract*—We use a 2D electrothermal continuum model that includes ion transport via diffusion and thermodiffusion to study the switching process of a device showing unipolar switching. We examine the influence of thermodiffusion on this unipolar switching process. Our theoretical investigation indicates that the unipolar operation cannot be described based on diffusion and thermodiffusion, in contrast to the proposal in literature.**

Keywords—unipolar resistive switching, memristive device, valence change mechanism, thermodiffusion

I. Introduction

A key component in the description of the switching mechanisms of bipolar metal-oxide-metal memristive devices is the redistribution of oxygen vacancies axially along the direction of the electrical current [1]. Aside from that, radial effects may also play a role in the switching characteristics. For a unipolar device, Strukov et al. proposed that the switching could be explained by radial thermodiffusion [2]. In this description, a temperature gradient leads to oxygen vacancy transport inwards towards a hotspot during the SET process, while the RESET process is characterized by elevated temperatures but with a low gradient, which causes the vacancies to diffuse back outwards. However, Strukov et al. assumed static temperature profiles for SET and RESET and a dynamic model supporting this idea is not available yet. It was further proposed that thermodiffusion governs the electroforming process for bipolar switching cells [3, 4]. For TaOx devices, however, we showed using dynamically calculated temperature profiles that thermodiffusion alone cannot explain the oxygen vacancy concentration measured after electroforming, even with the assumption that a conductive filament already exists [5].

II. Setup of the Simulation Model

In Fig. 1, a sketch showing the structure of the simulated device is presented. A voltage or current is applied to the top TiN electrode (red line), while the bottom TiN electrode is grounded (black line). The temperature at the bottom of the SiO_2 substrate (blue line) is fixed at $T = T_{\mathrm{amb}} = 293.15$ K. All other exterior interfaces of the device are thermally insulated. The radius of the top electrode is smaller than the radius used for the other layers to produce a radial temperature gradient. Oxygen vacancies are confined to the TaO_x layer and initially uniformly distributed at a concentration of $c_{\mathrm{V_O}} = 10^{25}\ \mathrm{m^{-3}}$.

Supported by funding from the DFG (SFB 917) and from the NEUROTEC project of the BMBF (grant no. 16ME0398K and 16ME0399).

XXX-X-XXXX-XXXX-X/XX/$XX.00 ©20XX IEEE

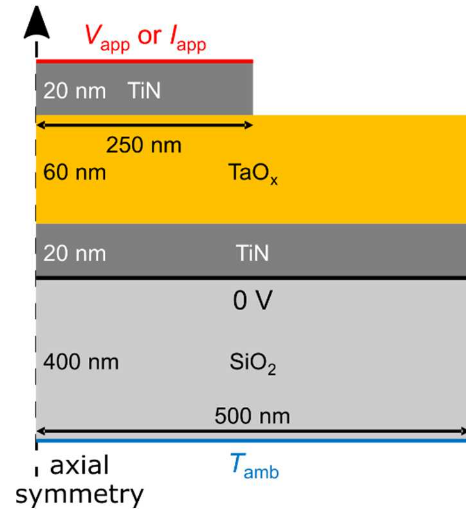

Fig. 1. Schematic overerview of the simulated device, including the boundary conditions.

The model comprises three equations for the three state variables: a static electric current continuity equation for the electric potential V, a time-dependent heat transfer equation for the temperature T, and a continuity equation for the concentration of oxygen vacancies $c_{\mathrm{V_O}}$. As the model does not include oxygen exchange at interfaces, the calculation of the vacancy concentration is limited to within the oxide, i.e., the TaO_x layer. In contrast, the temperature is calculated in the whole device. Meanwhile, the electric potential is calculated in the top electrode, the oxide, and the bottom electrode, but not in the substrate.

The equation governing the transport of ions, in this case oxygen vacancies, has the form:

$$\frac{\partial c_{\mathrm{V_O}}}{\partial t} = -\frac{1}{ze}\nabla\cdot\mathbf{J}_{\mathrm{V_O}} = \nabla\cdot\left(D\nabla c_{\mathrm{V_O}} + D_{\mathrm{T}} c_{V_O}\nabla T\right) \quad (1)$$

The ionic current density $\mathbf{J}_{\mathrm{V_O}}$ is composed of a part for diffusion $\mathbf{J}_{\mathrm{V_O,F}}$ and a part for thermodiffusion $\mathbf{J}_{\mathrm{V_O,S}}$. Here, diffusion stands for Fick diffusion along concentration gradients $\nabla c_{\mathrm{V_O}}$, while thermodiffusion is also called Soret diffusion and acts along temperature gradients ∇T. The two parts of $\mathbf{J}_{\mathrm{V_O}}$ can be individually written as:

$$\mathbf{J}_{\mathrm{V_O,\,F}} = -zeD\nabla c_{\mathrm{V_O}} \tag{2}$$

$$\mathbf{J}_{\mathrm{V_O,\,S}} = -zeD_{\mathrm{T}}c_{\mathrm{V_O}}\nabla T \tag{3}$$

with the charge number z, the elementary charge e, the diffusion coefficient D, and the thermodiffusion coefficient D_{T}, where:

$$D = D_0 \exp\left(-\frac{\Delta H}{k_{\mathrm{B}}T}\right)\cdot\left(1-\frac{c_{\mathrm{V_O}}}{c_{\mathrm{V_O,\,max}}}\right) \tag{4}$$

and D_{T} can be derived from D by multiplication with the Soret factor S_{T}:

$$D_T = S_T \cdot D = -\frac{\Delta H}{k_{\mathrm{B}}T^2}\cdot D \tag{5}$$

The maximum concentration of oxygen vacancies is set to $c_{\mathrm{V_O,\,max}} = 10^{28}\ \mathrm{m^{-3}}$, k_{B} is the Boltzmann constant, and ΔH is the activation enthalpy for oxygen vacancy transport. Unless otherwise noted, a value of $\Delta H = 0.8$ eV is chosen.

In our model, the description of ion transport does not include drift since the oxygen vacancies are assumed to be electrically neutral. As a result, only thermal effects directly influence the vacancy transport. By choosing the sign of the Soret factor, the direction of ionic current induced by thermodiffusion can be selected. The negative sign in (5) means that oxygen vacancies are drawn towards areas with higher temperatures, which is corroborated by [6].

The electric potential is given by:

$$\nabla\cdot\mathbf{J} = -\nabla\cdot(\sigma\nabla V) = 0 \tag{6}$$

where $\mathbf{J}$ is the electric current density and σ is the electrical conductivity. Within the oxide, the conductivity is modeled as:

$$\sigma_{\mathrm{TaO_x}} = \sigma_0 \cdot \frac{c_{\mathrm{V_O}}}{c_{\mathrm{V_O,\,max}}}, \quad \sigma_0 = 7.5\cdot 10^4\ \frac{\mathrm{S}}{\mathrm{m}} \tag{7}$$

and therefore, shows a linear dependence on the oxygen vacancy concentration.

Finally, temperature profiles are calculated via:

$$\rho C_p \frac{\partial T}{\partial t} = \nabla\cdot(\kappa\nabla T) - \mathbf{J}\cdot\nabla V \tag{8}$$

using the density ρ, the specific heat capacity C_{p}, and the thermal conductivity κ. Joule heating is included with the term $-\mathbf{J}\cdot\nabla V = \mathbf{J}\cdot\mathbf{E}$, where $\mathbf{E}$ is the electric field.

The material parameters for the simulated device, which are taken from the Supporting Information of [6], are summarized in Table I.

TABLE I. LIST OF MATERIAL PARAMETERS

	TiN	TaO_x	SiO_2
$\sigma\ \left[\frac{\mathrm{S}}{\mathrm{m}}\right]$	$5\cdot10^6$	See definition	-
ε_{r}	4	22	-
$\kappa\ \left[\frac{\mathrm{W}}{\mathrm{m\cdot K}}\right]$	5	4	1.4
$C_{\mathrm{p}}\ \left[\frac{\mathrm{J}}{\mathrm{kg\cdot K}}\right]$	545	174	730
$\rho\ \left[\frac{\mathrm{kg}}{\mathrm{m^3}}\right]$	5210	8200	2200

III. SIMULATED SWEEP

In Fig. 2, the *I-V* curves resulting from applying voltage- or current-controlled sweeps as visualized in Fig. 3 are presented. Irrespective of the starting polarity, the first leg leads to an increase in the electrical conductance of the device caused by a higher oxide conductivity, with no notable further changes during the rest of the sweep. This increase in the electrical conductivity of the oxide layer is equivalent to a SET operation, which can thus occur with both polarities. In the current-controlled sweeps, the SET coincides with a region of the *I-V* curve exhibiting S-type negative differential resistance that is caused by the lowered oxide resistivity. The unipolar nature of the SET is a consequence of the ionic motion being temperature driven.

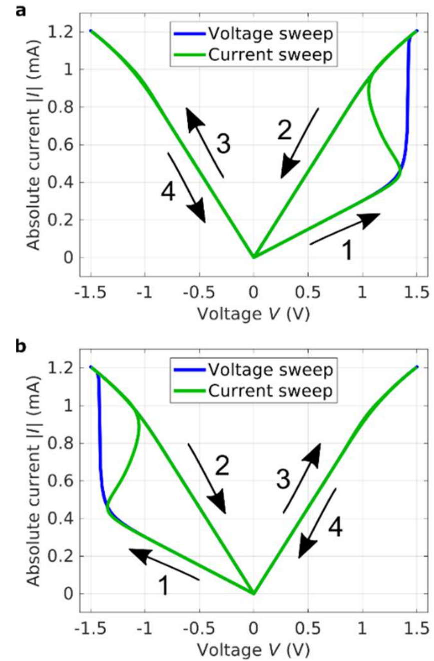

Fig. 2. Characteristics of voltage- and current-controlled *I-V* sweeps as given in Fig. 3. The numbered arrows highlight the path taken during the sweep. (a) Starting with a positive bias. (b) Starting with a negative bias.

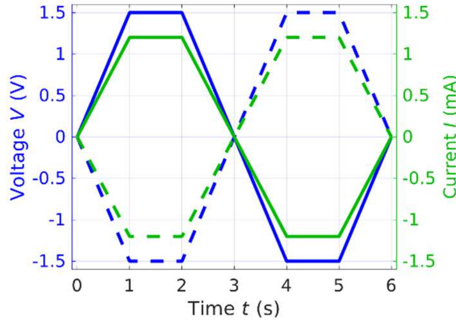

Fig. 3. Voltage or current applied during the *I-V* sweeps used in Fig. 2. The solid lines correspond to Fig. 2(a) and the dashed lines correspond to Fig. 2(b).

Fig. 4 and Fig. 5 illustrate how the SET process happens as feedback between Joule heating and ionic migration. The electrical conductivity is higher in the filament, causing the temperature gradient to the surrounding oxide to increase and more ions to move to the center, which results in a positive feedback. On the other hand, there is no RESET as the temperature is highest in the filament and the driving force is directed towards the center, thereby stabilizing the filament. As a result, unipolar switching is not possible since elevated temperatures cannot be achieved with low temperature gradients due to the device geometry.

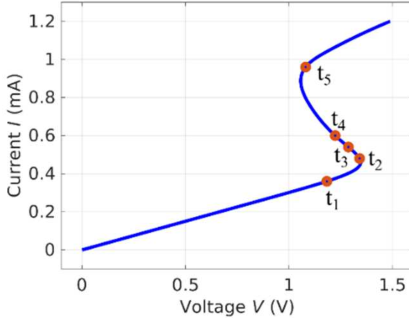

Fig. 4. *I-V* curve of a current-controlled *I-V* sweep identical to the first leg of the current sweep in Fig. 2(a). The times t_1 to t_5, at which the snapshots in Fig. 5 are taken, are marked by labeled red dots.

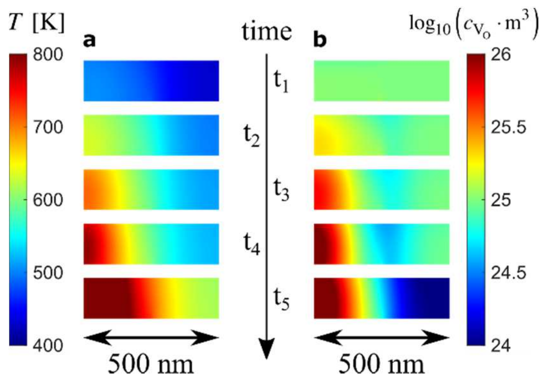

Fig. 5. (a) 2D snapshots of the temperature *T*. (b) 2D snapshots of the oxygen vacancy concentration $c_{\mathrm{V_O}}$. The corresponding points on the *I-V* curve are highlighted in Fig. 4. Each snapshot covers the entire oxide layer. The radial temperature gradient coincides with a radial transport of vacancies $\mathrm{V_O^x}$ towards the center of the device.

IV. VOLATILITY OF SWITCHING

The SET process observed in Fig. 2 is non-volatile, as the device stays well-conducting in the second half of the sweep. In Fig. 6, this is expanded to activation enthalpies ΔH of 0.6 eV and 1 eV, showing non-volatility in these cases, too. However, for $\Delta H = 1$ eV, the SET only occurs after the peak voltage of 1.5 V has been reached. Throughout this section, a voltage-controlled sweep starting with positive bias is used, with the applied voltage shown in Fig. 3 as a solid blue line.

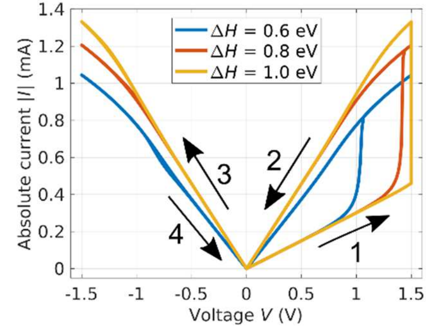

Fig. 6. *I-V* curves during a voltage-controlled sweep as indicated by the numbered arrows up to a peak voltage of 1.5 V for different activation enthalpies ΔH.

The SET behavior for $\Delta H = 1$ eV is more clearly visible in Fig. 7, where the maximum temperature gradually increases while the applied voltage stays constant at $V = 1.5$ V for $1\,\mathrm{s} \leq t \leq 2\,\mathrm{s}$. In the other cases, the switching event coincides with an abrupt temperature increase.

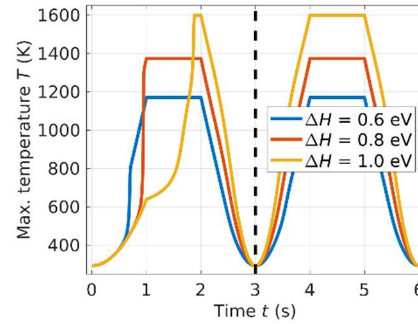

Fig. 7. Maximum device temperatures when using the same voltage-controlled *I-V* sweep as in Fig. 6. A vertical black dashed line marks the midpoint of the sweep where $V = 0$ V.

A look at the maximum concentration of oxygen vacancies in Fig. 8 reveals that after an initial increase defining the SET, it stays elevated for the rest of the sweep. As the absolute applied voltage is lowered after $t = 2$ s and after $t = 5$ s, the concentration further increases despite falling temperatures and consequently lower temperature gradients. While these gradients are the driving force of thermodiffusion, the Soret factor has a proportionality of $S_{\mathrm{T}} \propto T^{-2}$ that also must be considered. At elevated temperature, the equilibrium between diffusion and thermodiffusion is therefore shifted away from the latter. With falling temperatures, a rebalancing of the equilibrium occurs until the temperature is low enough to inhibit ion transport. For an activation enthalpy of 0.6 eV, the increase of $c_{\mathrm{V_O}}$ after $t = 2$ s and $t = 5$ s is immediately followed by a decrease due to enhanced low temperature ion mobility. As a critical filament temperature exists where thermodiffusion is maximized in relation to diffusion, there is

an overshoot in the maximum vacancy concentration during SET. This is most visible for $\Delta H = 1$ eV because of the gradual temperature increase.

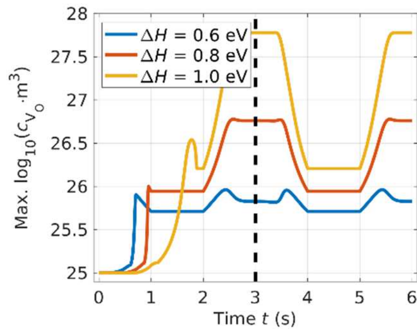

Fig. 8. Maximum c_{V_O} in the TaO_x layer during the same *I-V* sweep as used in Fig. 6. The point in the sweep at which $V = 0$ V is marked by a vertical black dashed line.

Ion mobility strongly depends on the activation enthalpy ΔH, so that by lowering its value, volatile switching can be induced. Conversely, for high enthalpies and a fixed peak voltage, oxygen vacancy transport is severely limited. According to the *I-V* curves in Fig. 9, a non-volatile SET occurs neither for $\Delta H = 0.3$ eV nor for $\Delta H = 1.1$ eV.

Fig. 10 shows that for $\Delta H = 0.3$ eV, except for high temperatures where the Soret factor is reduced, the maximum value of c_{V_O} closely follows the maximum temperature as the ion mobility stays high regardless of temperature. When the voltage reaches 0 V, with temperatures at ambient level, the initial uniform vacancy distribution is restored. By contrast, non-volatile behavior is evident for an activation enthalpy of 1.1 eV. However, due to the limited voltage, the maximum temperatures are insufficient for a complete SET. Instead, in each half cycle, c_{V_O} increases slightly while the absolute voltage is at its peak.

In summary, when lowering ΔH, the ionic mobility gets high enough to promote ion diffusion also at lower temperatures. In this case, a dynamic equilibrium evolves between diffusion and thermodiffusion, so that the filament is dissolved as soon as the applied voltage is removed.

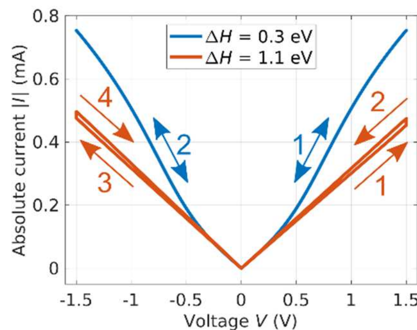

Fig. 9. For activation enthalpies of 0.3 eV and 1.1 eV, there is no non-volatile switching when the peak voltage of the voltage-controlled *I-V* sweep is fixed at 1.5 V. Color-coordinated numbered arrows show the path taken in each case.

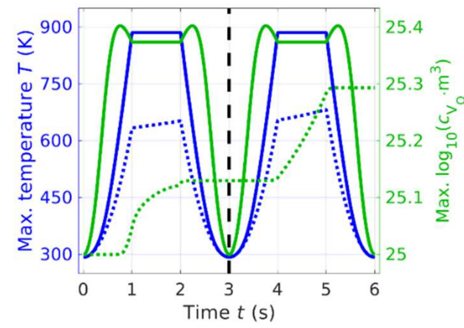

Fig. 10. Maximum device temperatures (blue) and maximum c_{V_O} in the TaO_x layer (green) for the activation enthalpies used in Fig. 9. Solid lines: $\Delta H = 0.3$ eV. Dotted lines: $\Delta H = 1.1$ eV.

For moderately high ΔH where the ion transport is inhibited at lower temperatures, the retention of the filament is vastly improved, but as discussed before, a dissolution of the filament by RESET is also not possible. In the case of further increased ΔH, the ionic mobility stays low even at elevated temperatures.

Conclusion

After having verified the unipolar nature of the simulated switching, which is limited to a single set event in the non-volatile case, we varied the activation enthalpy ΔH, allowing for both volatile and non-volatile switching. As it turns out, a RESET driven purely via diffusion and thermodiffusion is only possible in the volatile case. However, this does not constitute actual resistive switching as the system is constantly in equilibrium.

References

[1] R. Waser, R. Bruchhaus, and S. Menzel, "Redox-based resistive switching memories," in "Nanoelectronics and information technology", 3rd ed., R. Waser (ed.), Wiley-VCH, pp. 683-710, 2012.

[2] D. B. Strukov, F. Alibart, and R. S. Williams, "Thermophoresis/diffusion as a plausible mechanism for unipolar resistive switching in metal-oxide-metal memristors," Appl. Phys. A, vol. 107, no. 3, pp. 509–518, 2012.

[3] S. Kumar, Z. Wang, X. Huang, N. Kumari, N. Davila, J. P. Strachan, D. Vine, A. L. D. Kilcoyne, Y. Nishi, and R. S. Williams, "Conduction channel formation and dissolution due to oxygen thermophoresis/diffusion in hafnium oxide memristors," ACS Nano, vol. 10, no. 12, pp. 11205-11210, 2016.

[4] Y. Ma, J. M. Goodwill, D. Li, D. A. Cullen, J. D. Poplawsky, K. L. More, J. A. Bain, and M. Skowronski, "Stable metallic enrichment in conductive filaments in TaO_x-based resistive switches arising from competing diffusive fluxes," Adv. Electron. Mater., vol. 5, no.7, pp. 1800954, 2019.

[5] T. Heisig, K. Lange, A. Gutsche, K. T. Goß, S. Hambsch, A. Locatelli, T. O. Menteş, F. Genuzio, S. Menzel, and R. Dittmann, "Chemical structure of conductive filaments in tantalum oxide memristive devices and its implications for the formation mechanism," Adv. Electron. Mater., vol. 8, no. 8, pp. 2100936, 2022.

[6] S. H. Lee, J. Moon, Y.J. Jeong, J. Lee, X. Li, H. Wu, and W. D. Lu, "Quantitative, dynamic TaO_x memristor/resistive random access memory model," ACS Appl. Electron. Mater., vol. 2, no. 3, pp. 701-709, 2020.

[7] J. M. Goodwill, G. Ramer, D. Li, B. D. Hoskins, G. Pavlidis, J. J. McClelland, A. Centrone, J. A. Bain, and M. Skowronski, "Spontaneous current constriction in threshold switching devices," Nat. Commun., vol. 10, no. 1628, 2019.